

**BABEȘ - BOLYAI UNIVERSITY
FACULTY OF PHYSICS**



**DETECTION AND ANALYSIS OF POLLUTANTS USING SPECTROSCOPIC
METHODS ASSISTED BY PLASMONIC NANOSTRUCTURES**

- Doctoral thesis summary –

by

DANIELA SIMONA ȚÎRA

**Scientific Advisor
Prof. Dr. Simion Aștilean**

**Cluj-Napoca
2015**

Contents

Introduction.....	5
-------------------	---

PART I

GENERAL ASPECTS ON PHYSICAL AND CHEMICAL PROPERTIES AND APPLICATIONS OF PLASMONIC NANOPARTICLES IN SPECTROSCOPIC RESEARCHES

Chapter 1	10
Physical and chemical properties of plasmonic nanoparticles.....	10
1.1 Introduction.....	10
1.2 Electronic structure.....	11
1.3 Plasmonic resonance.....	13
1.4 Luminiscence properties.....	24
1.5 Chemical properties.....	26
1.6 Conclusions	30
References.....	32
Chapter 2.....	35
Methods of spectroscopic analyssis using plasmonic nanoparticles.....	35
2.1 Surface plasmon resonance spectroscopy.....	35
2.2 Fluorescence spectroscopy.....	41
2.2.1 The phenomenon of fluouescence.	41
2.2.2.Detection of molecules based on fluorescence	52
2.2.3 The interaction between metallic nanoparticles and fluorophore.....	54
2.3 Raman and SERS spectroscopy.....	60
2.3.1. Raman effect.	60
2.3.2. SERS effect: Surface-Enhanced Raman Scattering	64
2.3.3. Raman and SERS spectroscopy	66
2.4 Conclusions	68
References.....	69

PART II
PERSONAL CONTRIBUTIONS ON DETECTION OF POLLUTANTS USING
SPECTROSCOPIC METHODS ASSISTED BY PLASMONIC NANOPARTICLES

Chapter 3.....	72
Detection of Zn²⁺ ions in water based on the „turn-on” fluorescence method.....	72
3.1 Introduction	72
3.2 Experimental section.....	73
3.3 Results on detection of Zn ²⁺ ions in water based on the „turn-on” of the fluorescence of RhB molecules	74
3.4 Conclusions.....	80
References.....	81
Chapter 4.....	83
Detection of organic pollutants in water by SERS method.....	83
4.1 Introduction	83
4.2 Experimental section	85
4.3 Results on detection of methylene blue and basic fuchsin using SERS and network gold nanowires as a plasmonic substrate.....	87
4.4 Conclusions.....	95
References	96
Chapter 5.....	98
Simulations of localized plasmonic resonances in gold nanoparticles chains.....	98
5.1 Introduction	98
5.2 Theoretical part: FDTD method.....	99
5.3 Experimental section: synthesis and assembly of gold nanoparticles.	101
5.4 Comparison with experimental spectra and discussion of results.....	102
5.5 Theoretical calculation of position, shape and of electromagnetic field of plasmonic resonances generated by nanoparticles chains.....	106
5.6 Conclusions.. ..	111
References.....	112
Chapter 6.....	114
Final conclusions and perspectives.....	114
6.1 Final conclusions.....	114
6.2 Perspectives of the researches presented in thesis.....	115
6.3 Publications and participations at conferences.....	116
6.4. Acknowledgments.....	118

ANNEX

Annex 1	119
Spectroscopic equipment.....	119
1. The spectrophotometer UV-vis Jasco V530	119
2. The spectrofluorimeter Jasco FP 6000.....	121
3. The portable Raman spectrometer (Ocean Optics)	123
Annex 2	126
Methods and techniques of obtaining nanostructure substrates used in plasmonic senzoristical	126
1. Bottom-up techniques	126
2. Top-down techniques.....	130
References.....	135

Key words: metallic nanoparticles, plasmonic resonance, detection, analytes, fluorescence, fluorescence quenching, “turn-on” fluorescence, Raman effect, SERS, FDTD simulations

INTRODUCTION

„Detection and analysis of pollutants using spectroscopic methods assisted by plasmonic nanostructures” consists of two parts, the first one relying on literature and having a monographic character. The second part of the thesis contains original contributions connected with the experimental and theoretical studies I made and the results obtained which led to the accomplishment of the objective presented above.

Chapter 1 presents noble metal nanoparticles and their electronic, optic și chemical properties, putting an accent on surface plasmon resonance. There are the main ideas and scientific theories which explain the plasmon resonance phenomenon (Mie’s theory, Gans’ theory and Maxwell-Garnet’s theory) and offer adequate explanations of the different effects observed, like the colour of the colloids, the way the dimensions of the metal influence the physical and chemical properties of the nanoparticles, compared with the properties of the individual atoms or macroscopic metals.

Chapter 2 presents the main spectroscopic methods used for the investigation of the interaction between the molecules and plasmonic nanoparticles: the surface plasmon resonance spectroscopy, the fluorescence spectroscopy, Raman and SERS spectroscopy.

Chapter 3 presents the detection of zinc ions in water using the „turn-on” fluorescence method. First we used gold nanoparticles of about spherical shape and a diameter of approx. 18 nm as a substrate which quenches the fluorescence of Rhodamin B molecules adsorbed on the surface. The nanoparticles were obtained using the Turkevich-Frens method and were characterized using the extinction UV-vis measurements and the transmission electron microscopy (TEM). We demonstrated that the presence of the gold nanoparticles yield a strong quenching of the fluorescence of the RhB molecules through the fluorescence resonance energy transfer (FRET). On the other hand, the presence of zinc ions (zinc acetate) produced a „turn-on” fluorescence phenomenon to the RhB molecules due to the release of the RhB molecules of the nanoparticles surface by the zinc ions.

Chapter 4 presents the results of molecular detection using SERS method. We proposed a new method of obtaining gold nanostructures of irregular form which is a suitable substrate for SERS. We demonstrated that the addition of gold colloid (prepared following the standard method, Turkevich-Frens) with zinc acetate at room temperature, generate network-like gold nanostructures through association of the nanoparticles and their fusion. Plasmonic resonances of the network-like nanowires were recorded using extinction UV-vis-NIR spectroscopy, their spatial structure using transmission electronic microscopy (TEM), the crystal structure by X-ray diffraction (XRD) and their composition by EDX. The pollutants used as analytes were two organic dyes, basic fuchsin and methylene blue, intensively used in industry and medicine, often found in wastewater. SERS measurements were made in NIR, at 785 nm (NIR-SERS).

Chapter 5 presents the theoretical analysis of the plasmon resonances of gold nanoparticles organized in chain-like structures. We calculated the spectra of the electromagnetic near and far-field of these chain-like nanoparticles. This study is based on the FDTD method, i.e. numerically solving Maxwell's equations using differential methods and iteration over time. LSPR simulated spectra, corresponding to an increasing number of the nanoparticles in the chain, with a constant distance of 0.5nm in between them, were compared with the experimental extinction spectrum, obtained for a gold colloid having GNPs a diameter of about 20nm and the spectra obtained after addition of a Pluronic F127 solution, which induced a certain degree of aggregation of GNPs.

Chapter 6 contains final conclusions of the thesis, which highlights the importance and originality of the results obtained and the perspectives of continuing my studies. The final part presents the list of my scientific publications, based on the studies I made.

The thesis ends with two annex. The first one describes the technical characteristics of the equipment used in these studies. The second one, based on literature, reviews the modern methods of synthesis and fabrication of plasmonic nanoparticles and nanostructures.

PART I

GENERAL ASPECTS ON PHYSICAL AND CHEMICAL PROPERTIES AND APPLICATIONS OF PLASMONIC NANOPARTICLES IN SPECTROSCOPIC RESEARCHES

Chapter 1

Physical and chemical properties of plasmonic nanoparticles

1.1. Introduction

The first gold nanoparticles were apparently obtained in the early V- IV B.C. centuries in Egypt and China. One of the most famous uses of the use of metallic nanoparticles in ancient times is a museum object known as Lycurgus Cup, which is presumed to be manufactured by the romans in the V-th to IV-th century B.C.[1]. Down from the Middle Ages, the solutions containing gold nanoparticles suspended in water (gold colloids) were used for both aesthetic (as dyes for stained glass, ceramics and china) and curative purposes, in order to treat heart dysentery, epilepsy, tumours and for diagnosis of syphilis [1]. In the XIX-th century, Michael Faraday explained that the presence of some atomic gold aggregates gave the colloid its red colour. At the beginning of the XX-th century, the optical properties of spherical nanoparticles were explained theoretically for the first time by Mie [2].

1.2. Electronic structure

Metals present an electronic structure formed of energetic bands which are determined by quantum - mechanical rules. Particles with dimensions of a few nanometre display properties which represent a transition from those corresponding to the atomic scale to those corresponding to the macroscopic scale. Nanoparticles having a diameter smaller than 20 nm have properties that may be explained using the quantum - mechanical rules [3], which are valid when the de Broglie wavelength of the valence electrons is of the same order as the size of the particle itself.

The particles behave electronically as zero-dimensional quantum-dots. Free electrons „trapped” in such „metal boxes” have electronic stationary electronic waves with discrete energetic levels [1]. Therefore, the electronic energy spectrum of the noble metal particles presents a discreet shape, unlike the continuous energetic spectrum of the macroscopic metal.

1.3. Plasmonic resonance

The electronic properties of the clusters are close related to their optical properties. For instance, free electrons „trapped” in quantum boxes present a characteristic collective oscillation frequency of the plasma resonance, giving rise to the so-called plasmon resonance band [1]. This band, observed for noble metal particles having a diameter bigger than 2 nm is in the visible domain and its apparition is due to a phenomenon called surface plasmon resonance (SPR). This phenomenon represents a coherent oscillation of the electrons from the conduction band, which occupies energetic states above the Fermi level, due to the interaction with an electromagnetic field [4]. Inside the particle a magnified resonant field appears which, in the case of small particles, is uniform in the whole volume, while outside the particle, a dipolar field is produced. Therefore the scattered and absorbed light will be enhanced, and an amplification of the near-field at the particle surface can also be observed [5].

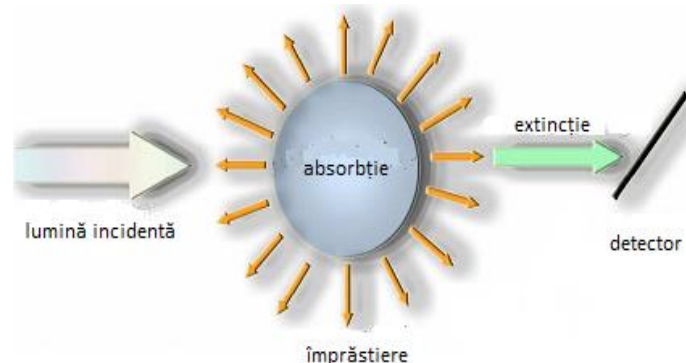


Fig.1. Schematic model of the interaction of the light with a nanoparticle, having as result absorption and scattering effects

The bandwidth, the size of the peak and the position of the absorbance maximum depend of the composition material of the particle, its dimensions and shape and the dielectric function of the surrounding medium [6]. In order to explain theoretically the way the surface plasmon resonance is influenced by those parameters, several theories were proposed: Mie’ theory, Gans’ theory and Maxwell – Garnett’ theory.

1.4. Luminescence properties

Photoluminescence of bulk gold and copper was first observed for the first time by Mooradian [7], which also established that the quantum efficiency of the photoluminescence from bulk noble metals is very small, usually about 10^{-10} . Later there have been studies on the effect of the surface roughness on the photoluminescence properties of noble metals. The luminescence efficiency was found to increase a few orders of magnitude on rough metal surfaces, phenomenon called *lightning rod effect*. The explanation of the photoluminescence was attributed to the radiative recombination of the electron – hole pair [8]. Electrons and holes can relax by scattering with phonons but then recombine radiatively to give rise to the observed luminescence.

1.5. Chemical properties

The use of metals in practical activities relies on the properties of their bulk form. Gold was used for manufacturing jewels, furnishings, coins and devices not only because their aesthetic properties, but also due to their low chemical reactivity and their great resistance to surface oxidation. The origin of chemical reactivity of the metals is related to their standard reduction potentials. Metals are usually electropositive and have a tendency to lose a bigger or smaller number of electrons, depending on the corresponding ionization energy. Reduction potential is thus correlated to the electropositive nature of the metals. When the dimensions are close to the nanoscale, though gold nanoparticles maintain their surface resistance to oxidation, the chemical reactivity increases and an increased catalytic behaviour may be observed, the nanoparticles being excellent catalysts, adsorbents and sensors.

Chapter 2

Methods of spectroscopic analysis using plasmonic nanoparticles

2.1 Surface plasmon resonance spectroscopy (SPR)

SPR spectroscopy is a modern technique of detection of different chemical and biological molecules. The detection based on the use of metallic surfaces use plasmons that appear on surfaces that separate a metal from a dielectric. Surface plasmons may be excited by electrons or photons. When the plasmons couple with a photon, the resulting particle is called polariton and the phenomenon of excitement of surface plasmons using light is called surface plasmon resonance (SPR). There are two types of surface plasmon resonance that may be used for detection:

a) surface plasmon resonance based on surface plasmons – conventional (unlocalised) polaritons (SPP) which propagate on plane surfaces;

b) surface localised plasmon resonance (LSPR), based on the existence of the plasmons which propagate on metallic structures characterised by dimensions of a few nanometres.

LSPR sensors functions using the excitement of plasmons that don't propagate and which exist on metallic nanoparticles' surfaces or around the nanoholes or nanocavities from thin metallic films. The spectral position and the size of LSPR depend on the dimensions, form, composition and local dielectric medium. The noble metal nanoparticles cause the apparition of LSPR when the frequency of the incident photons is resonant with collective oscillation of conduction electrons confined in the nanoparticle's volume [9], phenomenon that was presented in chapter 1. The collective oscillation frequency of the electrons existent in the nanoparticle, called localised surface plasmon resonance frequency (LSPR frequency) is sensitive to the changes of the local dielectric medium [10]. Typical researches based on LSPR detect the changes of the local medium measuring the shift of the wavelength LSPR though it is possible to detect these changes also by separation of the angles [11].

The simplest LSPR detection method is the ultraviolet and visible absorption spectroscopy (UV-vis). In this case we can measure the extinction spectrum (absorption and scattering) of nanoparticles, recording the dependence of the wavelength on the intensity of light that passes through the sample. Quantitative determinations are based on the Beer – Lambert law that has the following expression:

$$A = \varepsilon \cdot c \cdot d \quad (1)$$

where A – represents the measured absorbance, ϵ – the extinction coefficient, c – concentration of the sample and d – optical path through the sample.

2.2. Fluorescence spectroscopy

Fluorescence spectroscopy is based on the modifications of fluorescence characteristics produced by the presence of metallic nanoparticles.

Noble metal nanoparticles interact with fluorescent molecules existent nearby. This interaction often modifies the fluorescence intensity.

The fluorescence intensity may be decreased by a wide variety of processes. Such decreases in intensity are called *quenching* and can occur by different mechanisms. *Dynamic quenching* (collisional quenching) appear when the excited-state fluorophore is deactivated upon contact with some other molecules in solution, called quencher. Quenching may also be the result of the formation of a non-fluorescent complex between fluorophore and the quencher. When it occurs in the ground state and does not rely on diffusion or molecular collisions the process is called *static quenching*. Another important process that appears in the excited state is the resonance energy transfer (RET). This process appears when the emission spectrum of the fluorophore (called the donor) overlaps with the absorption spectrum of another molecule (called the acceptor) that does not need to be a fluorescent substance. RET does not involve neither an emission of light by the donor nor an emission from the donor being absorbed by the acceptor but a dipole-dipole interaction between the donor and the acceptor [12].

2.2.2. The detection of the molecules based on fluorescence

Unlike LSPR transmission spectroscopy which is based on the absorption of light, measured as a difference between the intensity of light that passes through a reference solution and the intensity of light that passes through the sample, fluorescence spectroscopy measures directly the intensity of light. There are many ways of detection of chemical or biological molecules based on fluorescence, determined by the fluorescence property which modifies after the interaction with the analyst: the intensity of light, the exciting spectrum or the anisotropy or the lifetime of the detected sample.

2.2.3. The interaction between metallic nanoparticles and the fluorescent molecules

The interaction between fluorescent substances and the metallic surfaces or nanoparticles may have multiple effects: the amplification or the decrease of the emission constant, the amplification of the fluorescence quantum yield of the chromophores having a small quantum

yield, the diminution of the fluorescence lifetime or the rapid orientation of the emitted radiation (usually isotropic) among certain directions. These effects do not appear because of the reflection of the emitted photons, they are the result of the interaction between fluorescent molecules and the free electrons inside the metal.

The fluorescence quenching produced by metallic nanoparticles may occur with two mechanisms: collisional quenching and resonant energetic transfer (RET). Both mechanisms represent non-radiative ways of transfer through the fundamental state, associated with modifications of spectral properties of the fluorophore.

2.3. Raman and SERS spectroscopy

2.3.1. Raman effect

The Raman effect appears when a molecular system is irradiated with monochromatic light from a laser. Suppose the laser emits light of a frequency ν_0 , and the energy of the photons, $h\nu_0$ is considerably less than the spacing between the ground and the first excited electronic energy levels, most of the photons will simply pass through the sample without interacting with its molecules. A small amount of light will be however scattered in all directions. An example of energy level diagram representing the energetic levels and the molecular scattering processes is represented in the next figure (Fig. 2).

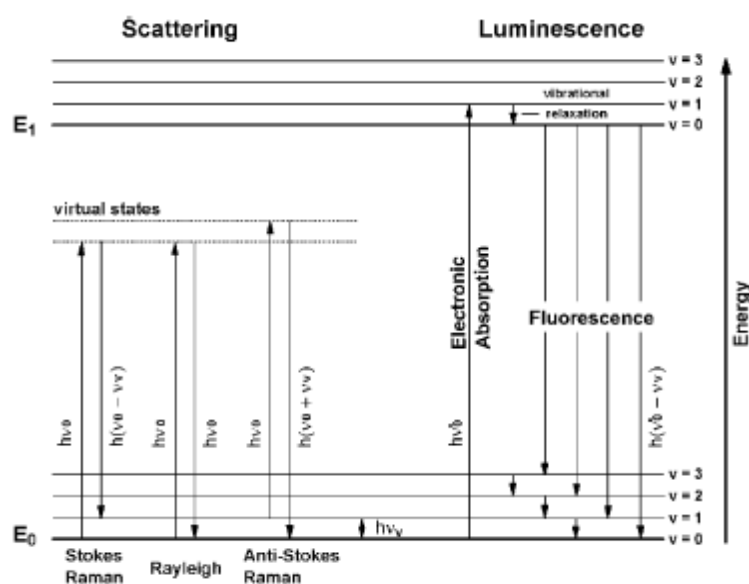


Fig. 2. Example of energy level diagram depicting, on the left-hand side, molecular scattering processes (Rayleigh and Raman) and, on the right-hand side, a photoluminescence process [13]

When the energy of the emitted light is the same as that of the incident light ($h\nu_0$) and the final state of the molecule is the same as the initial one ($E_0, \nu = 0$), the process is called *Rayleigh*

scattering. Other molecules, initially being in the ground vibrational state, \mathbf{E}_0 excited in the same virtual state, emit a lower energy upon decay than that of the excitation beam, equal to $\mathbf{h}(\mathbf{v}_0 - \mathbf{v}_v)$ during a process called *Stokes – Raman scattering*, which has as a result the apparition of lower frequency bands, called Stokes – Raman bands. If during the decay from the virtual state, the molecules emit light having an energy $\mathbf{h}(\mathbf{v}_0 + \mathbf{v}_v)$ which is $h\nu_v$ greater than that of the excitation beam, as they return to the final state $\mathbf{v} = \mathbf{0}$ of \mathbf{E}_0 , the process is called *anti – Stokes – Raman scattering*.

2.3.2. SERS effect: Surface-Enhanced Raman Scattering

In 1974 Fleischman and his co-workers noticed for the first time an amplification of the Raman signal scattered by the pyridine molecules adsorbed on the rough surface of a silver electrode [14].

In 1977, Jeanmaire and Van Duyne repeated the experiment and demonstrated that the intensity of the Raman scattered signal may be amplified by a couple of orders of magnitude when the molecules are placed on or near a roughened substrate of a noble material, obtained through repeated processes of oxide-reduction [15].

2.3.3. Raman and SERS spectroscopy

Spectroscopy based on Raman scattering amplified by the surface (SERS) is more frequently used because a SERS spectrum provides more information about the molecular structure and the surrounding medium than any other spectroscopic technique. Furthermore, due to those two mechanisms (electromagnetic and chemical) big amplifications (10^6) of the Raman signal are obtained in case the molecules are adsorbed on special metallic substrates, obtaining, in some cases, the detection of a single molecule [16].

Particular places, having adequate geometric configurations (edges, points, thresholds, flaws, holes or cavities) have Raman amplification factors of electromagnetic nature of $10^{11} - 10^{12}$ and may accomplish the detection of a single molecule [17].

The possibility of a single molecule detection is one of the most important advantage of SERS detection not only because of the very low limit of detection but also because of the fact that the molecule may be identified using its Raman spectrum.

PART II

PERSONAL CONTRIBUTIONS ON DETECTION OF POLLUTANTS USING SPECTROSCOPIC METHODS ASSISTED BY PLASMONIC NANOPARTICLES

Chapter 3

Detection of Zn²⁺ ions in water based on the „turn-on” fluorescence method

3.1. Introduction

The first two chapters reviewed the noble metal nanoparticles properties and the spectroscopic methods which exploit these properties. Due to the advantages that they present, we proposed to apply the described methods in order to detect different species of contaminants existent in water. In this chapter, we present a sensible nanosensor used for detection of Zn²⁺ ions in water [18]. The method is based on a strong quenching of the fluorescence of the dye ,

The concept is based on the substantial fluorescence quenching of Rhodamine B (RhB) molecules after dye adsorption onto GNPs surface. As a result of interaction between GNPs and Zn²⁺ ions, the RhB molecules are desorbed from the metal surface and the fluorescence recovered. We demonstrate that the system RhB-coated GNPs can be used as effective “turn-on” fluorescence sensor for precise dosing of Zn²⁺ ions in water.

3. 2. Experimental section

a) Chemicals. Tetrachloroauric acid (HAuCl₄ · 4H₂O, 99.99%), sodium citrate (C₆H₅Na₃O₇), and zinc acetate ((C₂H₃O₂)₂Zn) were obtained from Aldrich. Rhodamine B (C₂₈H₃₁CIN₂O₃) was purchased from Sigma.

b) Synthesis Of Gold Nanoparticles. Spherical GNPs were synthesized according to Turkevich-Frens method by aqueous reduction of HAuCl₄ with sodium citrate [19].

Sample preparation. Stock solutions of RhB (5·10⁻⁴ M) and zinc acetate (25·10⁻³ M) were prepared in ultrapure water and this solution was gradually diluted until a final concentration of 1.87·10⁻⁶ M. A similar procedure was used to analyse the fluorescence recovery of RhB as function of increasing concentrations of zinc acetate in RhB-coated GNPs solution. The TEM samples were obtained by drop-drying the solution on carbon-coated copper grids, followed by drying at room temperature.

c) Instruments. UV-Vis absorption measurements were carried out using a Jasco V-670 spectrophotometer. Fluorescence spectra were collected using a Jasco LP-6500

spectrofluorimeter. All fluorescence measurements were recorded in the right angle cell geometry (10 mm cell), under the same excitation conditions, specifically bandwidths of 1 nm in excitation and 3 nm in emission and excitation wavelength set at 532 nm. TEM images were obtained with a JOEL model JEM 1010 microscope.

3. 3. Results concerning the detection of Zn^{2+} ions in water using the “turn-on” fluorescence method of RhB molecules

a) Spectroscopic characterization of the interaction between the RhB molecules and gold nanoparticles

The UV-Vis absorption spectrum of RhB molecules in solution (see Fig. 3A, curve a) presents a strong absorption band at 556 nm, characteristic to the $\pi-\pi^*$ electronic transition of monomers, and a weak band at 520 nm assigned to the dimeric states of RhB molecules.

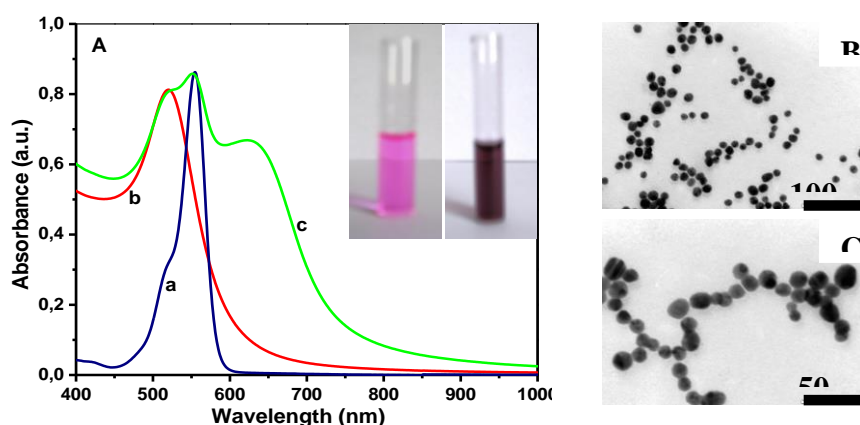


Fig. 3 . UV-Vis absorption spectra of RhB solution (a), GNPs solution (b), and 1:1 mixture between RhB and GNPs solutions (c). Inset shows the photographic images of RhB solution before and after mixing with GNPs. (B). TEM image of GNPs; (C). TEM image of RhB-coated GNPs [18].

The colloidal solution of citrate-capped GNPs exhibits a well-resolved extinction band at 521 nm (Fig. 3A curve b) assignable to LSPR of individual spherical nanoparticles of 18 ± 2 nm diameter, as given by TEM analysis (see representative TEM pictures in Fig. 3B). Upon adding 1 ml RhB solution of 10^{-5} M concentration to the same volume of colloidal solution (1ml), a new plasmonic absorption band at about 639nm is observed (Fig. 3A curve c). This new emerging band together with the drastic colour change of the mixture solution – from original red to violet blue (see insert in Fig. 3) represents the hallmark of electromagnetic coupling of nanoparticles with formation of small aggregates (Fig. 3A, curve c). The main plasmonic band decreases and

shifts slightly to red as result of dielectric changes around nanoparticles [20]. The induced aggregation of citrate-capped GNPs is further confirmed by TEM analysis. The TEM pictures recorded before (Fig. 3B) and after (Fig. 3C) addition of RhB molecules clearly prove the partial aggregation of GNPs in the form of linear and branched chains, as result of dye adsorption.

Next we studied the fluorescence of RhB molecules in the presence of GNPs. As fig. 4 shows, RhB molecules show a strong fluorescence emission band centred at 577 nm which exhibit good overlapping with the absorbance band of aggregated GNPs – a pre-requisite condition for an efficient resonance energy transfer.

Indeed, it is expected that the excited-state energy from the fluorophors to be transferred to the nanoparticle through a non-radiative process, named resonance energy transfer (RET) or FRET. The FRET can occur only when there is a sufficient overlap between the absorption band of acceptor (here GNPs) and the fluorescence band of donor (here RhB molecules) and the molecule are in close vicinity, as the efficiency of FRET depends on the inverse sixth power of the distance of separation between the donor and acceptor. This FRET occurs via an induced-dipole-dipole interaction when the dye molecule exchanges energy with the GNP of similar resonance wavelength without requiring of photon emission [21].

The fluorescence intensity of RhB is strongly reduced upon the addition of different volumes of GNPs, as seen in Fig. 4.

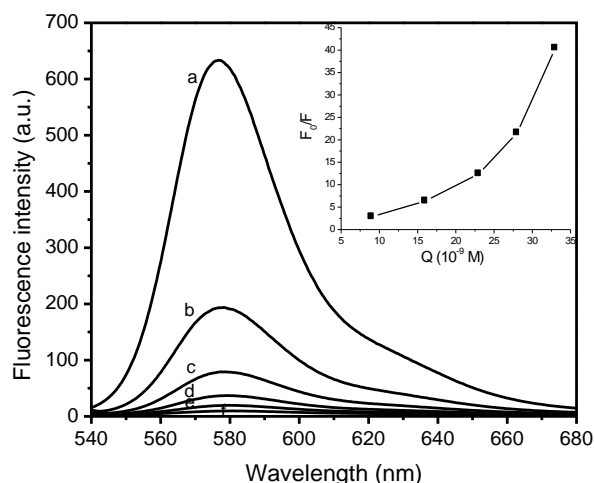


Fig.. 4. Evolution of normalized fluorescence spectra of RhB solution as function of increasing amounts of GNPs: 200 μ l (b), 400 μ l (c), 600 μ l (d), 800 μ l (e), and 1 ml (f). Spectrum (a) represents the fluorescence of RhB solution free of GNPs. The inset shows the relationship between (F_0/F) ratio and GNPs concentration. The spectra were normalized to fluorescence spectrum of free RhB solution (spectrum a). Excitation wavelength: 532 nm [18].

By plotting the ration (F_0/F) vs. GNPs concentration, where F_0 and F represent the fluorescence intensity of RhB solution in the absence and presence of GNPs, respectively, a sloping curve was obtained (see inset in Fig. 4), achieving thus some information about the quenching mechanism of RhB fluorescence. The obtained plot in our case is not linear, indicating that the RhB molecules exhibit a faster quenching than resulted from a pure static mechanism [12]. We should exclude the possibility of dynamic collisional quenching mechanism because of permanent and strong interaction existing between molecules and nanoparticles.

The deviation from linearity can be modelled by the extended model of classical Stern-Volmer equation presented bellow [29], where K represents the binding equilibrium constant, Q_{tot} is the total concentration of active sites on the nanoparticle quenchers and β is the dye fluorescence intensity factor ($\beta = F/c_{RhB}$):

$$\frac{F_0}{F} = 1 + \frac{KQ_{tot}}{\left(1 + \frac{KF}{\beta}\right)} \quad (2)$$

The upward deviation from the standard linear behaviour can be explained by the contributions of several factors, among them the fact that a fraction of RhB molecules are captured in between nanoparticles as result of aggregation. Therefore, it is conceivable that the rate of nonradiative decay of molecules located at the interstice between nanoparticles should be higher that of molecules adsorbed directly onto the surface of individual nanoparticles. Moreover, the spectra of RhB and GNPs aggregates overlap completely which in turn increases the energy transfer efficiency in the system. This could explain the accelerated static quenching as function of GNPs concentration and the existence of non-Förster resonance energy transfer mechanism from RhB molecules to GNPs [18].

b) Turn-On Fluorescence For Sensing Zn^{2+} Ions Based On Rhb-Coated Gnps System

Next, we evaluate the sensitivity in detection of Zn^{2+} by “turning-on” the fluorescence emission of RhB molecules in RhB-coated GNPs hybrid system.

As mentioned above, while the free RhB molecules are highly fluorescent in solution, the fluorescence emission of RhB adsorbed onto GNPs surface is quenched via energy transfer. However, as we can see in Fig. 5, in the presence of Zn^{2+} ions, the fluorescence intensity of RhB molecules recovers gradually with the increase of added Zn^{2+} ions. This means that RhB molecules are released from the GNPs’ surface, restoring their fluorescence and proving the successful demonstration of a “turn-on” fluorescence sensor for the detection of Zn^{2+} ions. The detachment of RhB molecules from the surface of gold nanoparticles is triggered by a stronger

affinity of Zn^{2+} cations toward gold surface and citrate corona, although the mechanism of detachment is not clear.

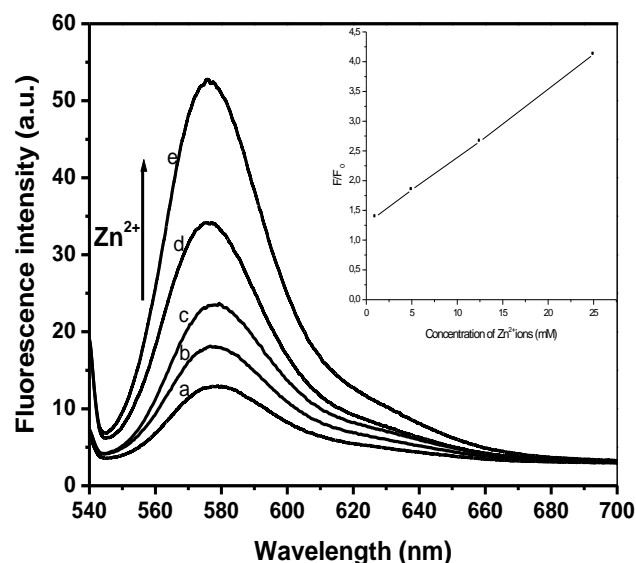


Fig.. 5. Recovery of fluorescence emission in RhB-coated GNPs system as function of Zn^{2+} ions concentration: 1mM (b), 5mM (c), 12.5mM (d) and 25 mM (e). The inset shows the linear plot of fluorescence ratio $(F_{on} - F_{off}) / F_0$ as a function of Zn^{2+} ions concentration, where F_0 is the fluorescence intensity of pure RhB solution (reference spectrum (f)), F_{off} is the “turn-off” fluorescence intensity corresponding to RhB-coated GNPs solution as recorded before adding Zn^{2+} ions (spectrum (a)) and F_{on} is the current “turn-on” fluorescence intensity of RhB-coated GNPs solution as measured at different concentrations of Zn^{2+} ions (spectra (b), (c), (d), and (e)). Excitation wavelength: 532nm[18].

We must mention that the fluorescence intensity of the „turn-on” fluorescence versus the Zn^{2+} concentration is a linear plot within a large domain of concentrations. (see inset in Fig. 5). The release of RhB molecules from the surface of GNPs after mixing RhB-coated GNPs with zinc acetate was studied by UV-vis spectroscopy and TEM analysis.

The extinction spectrum indicates a better spectral separation of the “fingerprint” band of free RhB molecules at 556 nm from the red-shifted plasmonic band corresponding to GNPs aggregate (see Fig 6, spectrum b). With increasing concentration of zinc ions added to solution, the LSPR bands increases also in intensity and features larger and larger aggregates [18].

The TEM image in Fig 4 shows GNPs aggregates which exhibit size and form particularly different relative to aggregates existing in solution before adding Zn^{+2} ions. In fact the addition of metallic ions modifies the ionic strength of colloidal solution and this induces accelerated aggregation as result of dramatic change in charge surface of GNPs after chemical displacement of RhB.

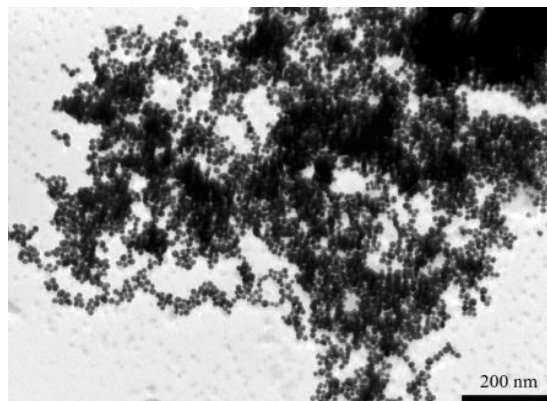
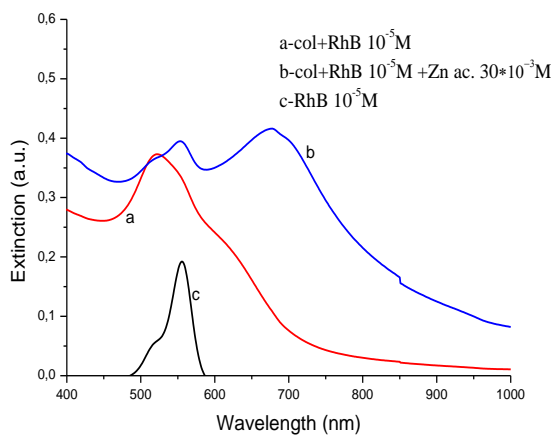


Fig.. 6. UV-Vis extinction spectra recorded before (curve a) and after (curve b) RhB molecules displacement from the surface of GNPs. The reference spectra of pure Zn acetate and RhB solutions are given in curve (c) and curve (d), respectively. Inset shows a representative TEM picture of GNPs aggregates produced after RhB displacement [18].

Chapter 4

Detection of organic pollutants in water using SERS method

4. 1. Introduction

The control of aquatic ecosystems, wastewater and potable water became an important challenge for the last decades since the amount of industrial pollutants increases every year. Particularly, the fast and sensitive detection of organic dyes in watercourses have attracted much attention in recent years because some synthetic dyes are quite toxic and harmful to people [22–24]. This is also the case of basic fuchsine and methylene blue, two organic dyes used in industry.

SERS is a highly specific and sensitive method for molecular identification as it enables an ultrasensitive detection, down to a single molecule, and provides structural information about the molecular species from their unique vibrational Raman finger- print [25–28].

The most critical challenge to perform a sensitive SERS measurement is therefore the design of a robust, well-defined, stable, low-cost, reproducible and highly efficient SERS substrates for trace detection of various pollutants.

In this study we propose a facile, rapid and low-cost method for SERS activation of spherical gold nanoparticles of 18 nm diameter by adding the zinc acetate solution into the gold nanoparticles dispersion. Stable colloidal network-like gold nanostructure is obtained at room temperature with the assistance of zinc ions. We demonstrate that the fabricated platform can operate as NIR-SERS substrate for monitoring trace amounts of organic dyes in aqueous solution, here basic fuchsine and methylene blue. The high sensibility, low-cost, quick response and NIR availability of the fabricated plasmonic architecture make it a promising candidate for applications in SERS detection of organic molecules [29].

4. 2. Experimental

a) Chemicals. Hydrogen tetrachloroaurate(III) trihydrate ($\text{HAuCl}_4 \cdot 3\text{H}_2\text{O}$, 99.99%), trisodium citrate ($\text{C}_6\text{H}_5\text{Na}_3\text{O}_7 \cdot 2\text{H}_2\text{O}$), zinc acetate ($(\text{C}_2\text{H}_5\text{O}_2)_2\text{Zn}$), methylene blue ($\text{C}_{16}\text{H}_{18}\text{ClN}_3\text{S}$) and p-aminothio-phenol (p-ATP) were obtained from Sigma–Aldrich. Basic fuchsine ($\text{C}_{20}\text{H}_{19}\text{N}_3 \cdot \text{HCl}$) was purchased from Merck.

Preparation of colloidal network-like gold nanostructures. The gold colloid was prepared following the Turkevitch–Frens method [30]. For gold nanostructures preparation, 500

mL colloidal solutions of spherical gold nanoparticles were incubated for 10 min at room temperature with 500 mL aqueous solution of zinc acetate ($15 \cdot 10^{-3}$ M).

c) Characterization methods. The LSPR spectra were measured in a 2 mm quartz cell using a Jasco V-670 UV–vis-NIR spectrometer with 1 nm spectral resolution. The TEM images were taken using a JEOL JEM 1010 transmission electron microscope (TEM). For TEM measurements the samples were prepared by placing a drop of colloidal dispersion onto carbon-coated copper grids and dried at room temperature. The crystal structure was characterized using a Shimadzu XRD 6000 diffractometer with Cu Ka radiation ($\lambda = 1.54 \text{ \AA}$). The elemental composition was conducted on a JEOL JSM 5600LV scanning electron microscope (SEM) equipped with an energy dispersive X-ray (EDX) detector with standard less elemental quantification in the INCA 200 software package (Oxford Instruments). The NIR-SERS measurements were recorded using a portable Raman spectrometer (Raman Systems R3000CN from Ocean Optics) equipped with a 785 nm diode laser coupled to a fibre optic probe of 100 mm core diameter. The laser power was set to 100 mW and the integration time to 30 s with a single accumulation for each measurement.

4. 3. Results concerning the detection of methylene blue and basic fuchsin using SERS and network gold nanowires as a plasmonic substrate

The formation of the colloidal network-like gold nanostructures was monitored by combining the UV–vis-NIR extinction spectroscopy, TEM images, XRD, EDX measurements and Raman spectroscopy. The prepared colloidal solution appears red-burgundy and the optical extinction spectrum exhibits a dominant plasmonic band at 520 nm (Fig. 7a) which represent the typical signature of the dipolar plasmon resonance of individual spherical gold nanoparticles with a mean diameter of 18 nm (Fig. 8A inset) [30, 31].

Immediately after the addition of zinc acetate solution into the gold nanoparticles dispersion the colour of colloidal solution changes from red-burgundy to blue. As the colour of gold nanoparticles is strongly dependent on their morphology, such colour evolution should be connected to the morphological transformation of gold nanoparticles, which evolve in solution from individual to interconnected nanoparticles. Analysis, this second, red-shifted band is consistent with a plasmonic resonance supported by interconnected gold nanoparticles into network-like nanostructures as presented in TEM images (Fig. 2A, B). 3.2. XRD and EDX characterization The crystalline structure of the nanomaterials is a critical

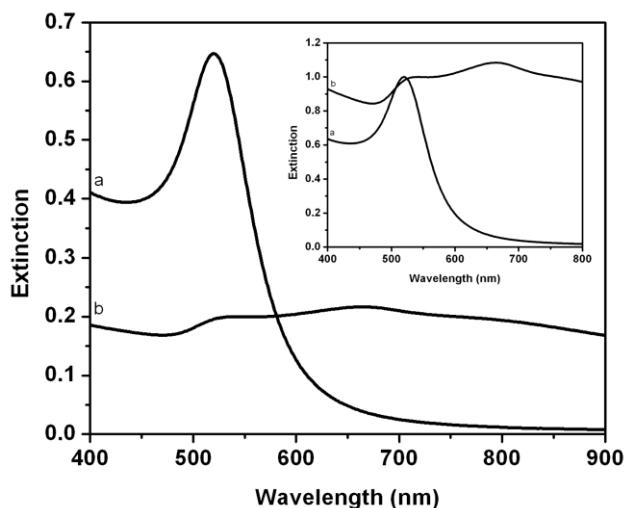


Fig. 7. UV–vis-NIR extinction spectra of colloidal gold nanoparticles: (a) before adding zinc acetate solution and (b) after adding zinc acetate solution. The inset shows the normalized corresponding extinction spectra [29].

The representative extinction spectrum demonstrating the change of gold nanoparticles morphology is depicted in Fig. 7b. Compared with the original spectrum of well-dispersed spherical gold nanoparticles, the plasmon resonant band at 520 nm was considerably suppressed and, in addition, a new broad band is evident with the maximum at 667 nm.

According to our subsequent TEM, this second, red-shifted band is consistent with a plasmonic resonance supported by interconnected gold nanoparticles into network-like nanostructures as presented in TEM images (Fig. 8A, B).

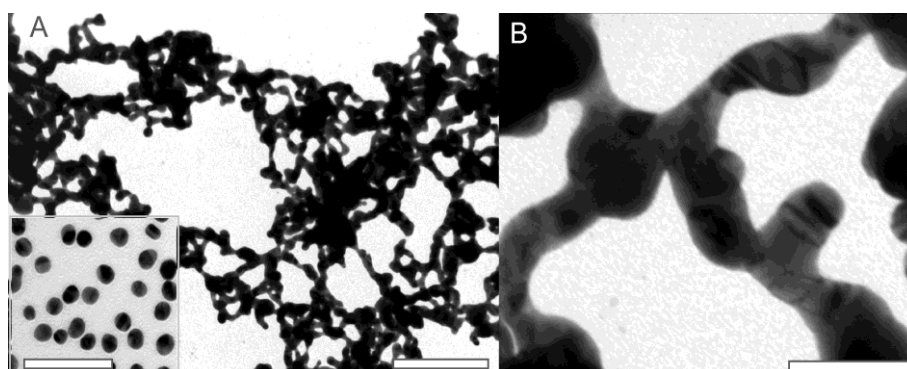


Fig. 8. (A) A representative TEM picture of the fabricated colloidal network-like gold nanostructures. (B) Zoom of the TEM image showing the gold network. The inset illustrates a representative TEM image of colloidal spherical gold nanoparticles. Scale bars: 200 nm for image A, 50 nm for image B and 100 nm for inset image respectively [29].

XRD and EDX characterization

The crystalline structure of the nanomaterials is a critical factor in understanding the formation of anisotropic nanostructures and, therefore in designing devices with desired function. Furthermore, the crystal morphology could also affect nanomaterials reactivity because of the differences in surface energy of different crystal faces. Therefore, in the next step of our study we characterized the crystalline structure of prepared nanostructures by X-ray diffraction (XRD) measurements.

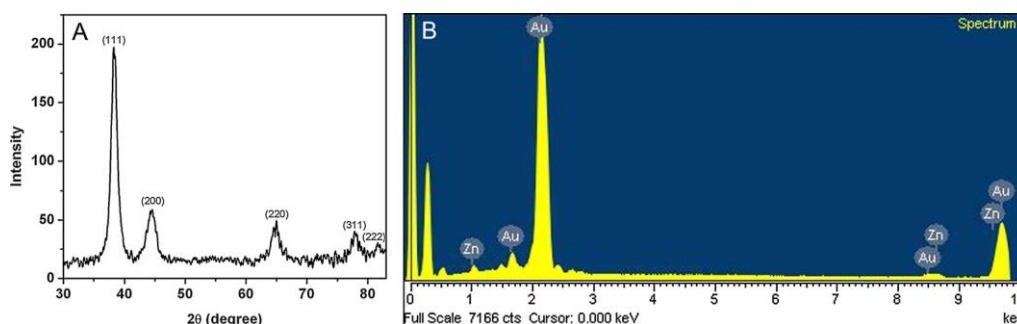


Fig. 9. (A) XRD Spectra of the network gold nanowires obtained. (B) EDX Analysis showing the high purity of gold (atomic percentage 95.48%) with infima traces of Zn (atomic percentage 4.52%) [29].

The XRD spectrum in Fig. 9A provides clear evidence for the crystalline structure of as-prepared gold networks. Energy-dispersive X-ray (EDX) analysis (Fig. 9B) shows the characteristic peaks for Au (2.12 keV and 9.71 keV) and for Zn (1.01 keV and 8.63 keV), confirming the presence of these two elements in the network-like nanostructures. However, the notable difference in intensity of peaks assigned to two elements, clearly demonstrates that the nanostructures fabricated in this study are made of high-purity gold (95.48% atomic percent) with only traces of Zn (4.52% atomic percent) [29].

Raman characterization

Beyond UV–vis–NIR extinction spectroscopy, TEM and XRD measurements, a proof of gold nanoparticles activation for SERS resulted also from Raman measurements.

Previous studies demonstrate the applicability of sodium citrate molecules used for nanoparticles stabilization as internal Raman probe [32–34]. Considering this the first assessment of the SERS activity of the fabricated network-like gold nanostructures was conducted using this molecule. As sodium citrate is a UV absorber any resonant or pre-resonant

contribution to the SERS effect is excluded. Comparative experiments between well-dispersed colloidal spherical gold nanoparticles and network-like gold nanostructures were carefully conducted to evaluate their SERS response under NIR excitation. Part a of Fig. 10A shows the SERS spectrum of citrate capped network-like gold nanostructures. For comparison, the Raman spectrum of solid sodium citrate is also shown in part b of Fig. 10A. The presence of the same spectral features in both Raman and SERS spectra clearly identify the presence of citrate molecules onto the gold network surface. The prominent band at 1018 cm^{-1} observed in the SERS spectrum corresponds to the C—O stretching of the tertiary alcohol [24–26]. The bands between 1300 and 1500 cm^{-1} are due to symmetric carboxylate stretching mode, and those between 800 and 1000 cm^{-1} are caused by C—COO and C—OH stretching modes [32–34].

The presence of a weakly bound citrate layer onto the gold nanostructure surface is crucial for their further applicability as SERS platforms because citrate molecules can be easily replaced by analytic molecules. This in turn allows the efficient adsorption of the analytes and simplifies the sample preparation. In this regard, in the next step of our work we selected para-aminothiophenol (p-ATP) as an external Raman analytic to form a self-assembled monolayer on the metal surface upon binding between thiol moiety and gold.

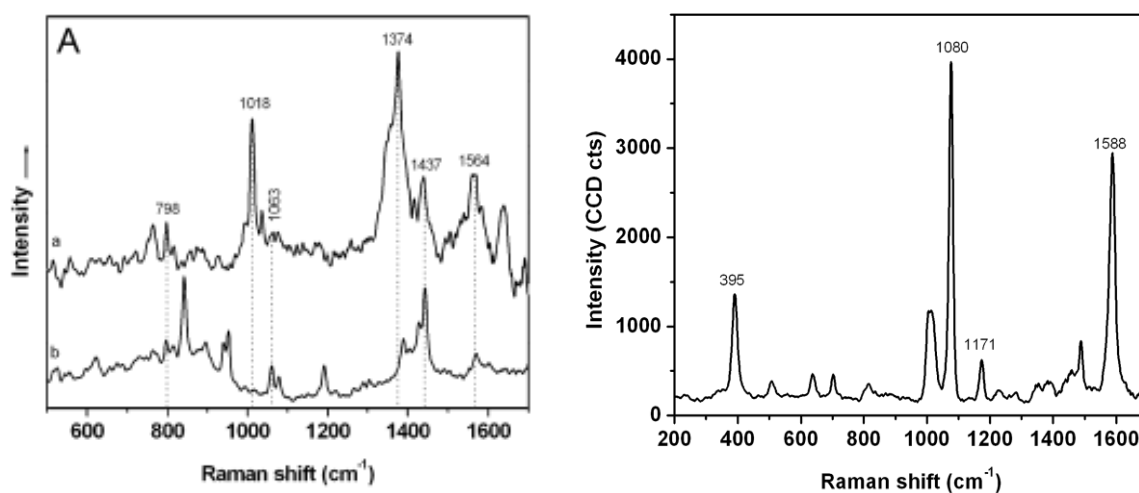


Fig. 10. (A) The NIR-SERS spectrum of citrate molecules adsorbed on network-like gold nanostructures (a) and the normal Raman spectrum of solid sodium citrate (b). (B) The NIR-SERS spectrum of $10 \cdot 10^{-6}$ M p-ATP molecules adsorbed on network-like gold nanostructures [29].

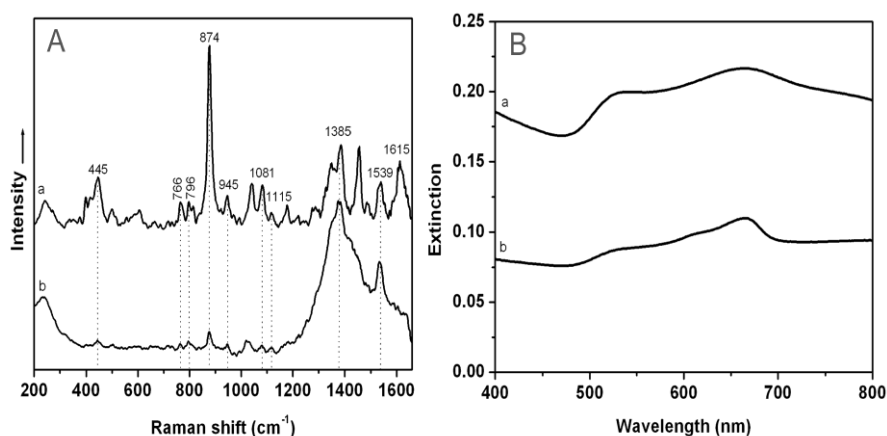
As shown in Fig. 10B, high-quality SERS spectrum of p-ATP was recorded under NIR laser excitation which clearly demonstrates that the citrate molecules used for nanoparticles stabilization does not hinder the adsorption of p-ATP molecules. Moreover, the SERS spectrum

of p-ATP in Fig. 10B does not show the citrate spectral features which indicate that the citrate molecules were replaced by p-ATP. In particular, the strong bands at 1080 cm^{-1} and 1588 cm^{-1} together with other two medium bands at 395 cm^{-1} and 1171 cm^{-1} are assigned to a1 vibration modes of p-ATP, namely C—S stretching vibration, C—C stretching mode, C—C—C bending vibration and C—H bending mode, according to literature [35, 36].

SERS application of network-like gold nanostructures

Based on the above results, it is therefore predictable that such SERS substrates could be applied in various aqueous environments, especially to capture and identify pollutants, pharmaceutical products or other chemicals. In view of such applications we demonstrate the feasibility of the fabricated network-like gold nanostructures to operate as NIR-SERS substrates for monitoring trace amounts of pollutants, here basic fuchsine and methylene blue. In Fig. 11A we acquired the NIR-SERS spectra of methylene blue molecules in solution at the final concentrations of $3 \cdot 10^{-6}$ and $5 \cdot 10^{-7}$ M. Characteristic bands of methylene blue molecules were achieved for both concentrations. In particular, the vibrational bands at 445, 1385, 1539 and 1615 cm^{-1} are assigned to C—N—C skeletal bending, in-plane C—H ring deformation, C—C asymmetric stretching and C—C ring stretching according to the literature [37,38].

To investigate the stability of the fabricated network-like gold nanostructures in the presence of methylene blue molecules we compared the optical extinction spectra of colloidal gold nanostructures before and after incubation with methylene blue. Fig. 11B shows the extinction spectra of colloidal gold nanostructures before (curve a) and after the addition of methylene blue solution (curve b). Compared with the original spectrum of colloidal gold nanostructures, a decrease of the plasmonic bands intensity with a concomitant red shift of 2 nm was observed in the presence methylene blue solution.



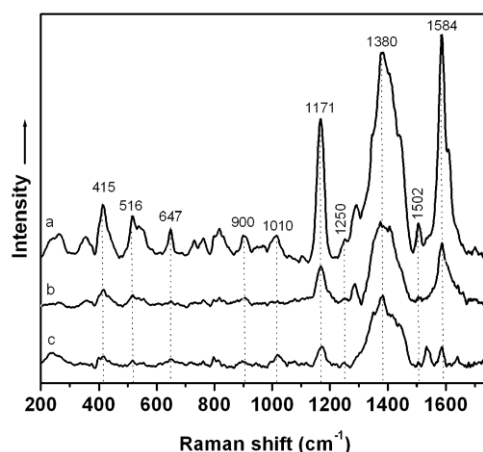


Fig. 11. (A) The NIR-SERS spectra of different concentrations of methylene blue molecules adsorbed on network-like gold nanostructures: (a) $3 \cdot 10^{-6}$ M, (b) $5 \cdot 10^{-7}$ M. (B) UV-vis-NIR extinction spectra of colloidal network-like gold nanostructures: (a) before adding methylene blue solution and (b) after adding methylene blue solution of $3 \cdot 10^{-6}$ M. (C) The NIR-SERS spectra of different concentrations of basic fuchsin molecules adsorbed on network-like gold nanostructures: (a) $2 \cdot 10^{-6}$ M, (c) $2 \cdot 10^{-7}$ M. (b) The NIR-SERS spectrum of $2 \cdot 10^{-6}$ M basic fuchsin molecules adsorbed on colloidal spherical gold nanoparticles[29].

According to our SERS analysis a possible explanation is that the methylene blue molecules immobilize on the gold network surface, leading to a change of the electrical charge on the nanostructures surface which consequently induces a decrease of the extinction bands intensity. The shift of the plasmonic bands could be connected with a change in the refractive index of the medium surrounding the nanostructures due to the adsorption of methylene blue molecules onto the gold network surface.

It is worth mentioning that our SERS platform is not limited to methylene blue molecules and other pollutants can be successfully detected at low concentrations. For example, in Fig. 12C parts a and c we acquired the NIR-SERS spectra of basic fuchsine molecules in solution at the final concentrations of $2 \cdot 10^{-6}$ and $2 \cdot 10^{-7}$ M. The spectra exhibit the characteristic vibrational bands of basic fuchsine. Therefore, the vibrational bands at 415, 1171, 1380 and 1584 cm^{-1} are assigned to the out-of-plane benzene ring deformation, C—H bending, N-phenyl stretching and in-plane ring stretching and bending according to the literature [39].

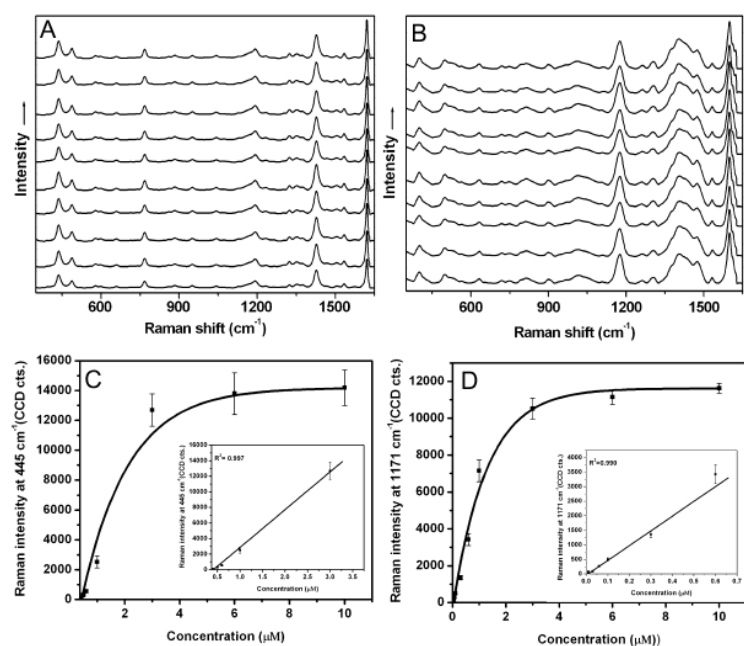


Fig. 12. The SERS spectra of: (A) methylene blue and (B) basic fuchsine at a concentration of $3 \cdot 10^{-6}$ M collected from different batches of gold substrates. Plots showing the correlation between the average intensity of the selected characteristic SERS bands and the concentration of probe molecules in solution: (C) methylene blue (445 cm^{-1}) and (D) basic fuchsine (1171 cm^{-1}). The insets show the linear relationship in the concentration ranges of 10^{-7} to 10^{-6} and 10^{-8} to 10^{-6} M for methylene blue and basic fuchsine, respectively [29].

The reproducibility of the SERS signal is a major requirement for any analytical applicability of a SERS platform. To check the reproducibility of the SERS signal, several samples were prepared by following the same protocol and the SERS spectra were collected under identical conditions. Fig. 12 A, B shows that the intensity, spectral position and the full width of the SERS bands are relatively constant from batch to batch for both molecules. The reproducibility of signal intensity was quantified by averaging the values of relative standard deviation (RSD) calculated for several selected Raman vibration bands. We found an average value of about 11% which can be considered in the range of typical RSD values for SERS measurements [40], indicating that our fabricated substrates are competitive for analytic applications.

To evaluate the limit of detection (LOD), the fabricated network-gold nanostructures were incubated with solutions of methylene blue or basic fuchsine of decreasing concentration (10^{-6} to 10^{-8} M) and examined for LOD under same experimental conditions in term of laser power and integration time. To certify the reliability of LOD values, the measurements were performed in triplicate, i.e., for each nominal concentration the SERS intensity was averaged

from measurements on three substrates. Fig. 12 C, D shows the average intensity of the selected SERS bands as function of methylene blue and basic fuchsin concentrations, respectively. The error bars in Fig. 12 C, D represent the calculated RSD for the variation of the signal intensity.

The insets in Fig. 12 C, D show a linear relationship in the concentration ranges of 10^{-7} to 10^{-6} and 10^{-8} to 10^{-6} M for methylene blue and basic fuchsin, respectively with a linear regression coefficient (R^2) of 0.99. From the linear calibration curve, we found the LOD of our SERS platform of $4 \cdot 10^{-7}$ M for methylene blue and $3 \cdot 10^{-8}$ M for basic fuchsin. The values of LOD indicate that the fabricated network-gold nanostructures are promising SERS platforms for quantitative analysis of organic pollutants [29].

Chapter 5

Simulations of localized plasmonic resonances in gold nanoparticles chains

5. 1. Introduction

Experimental studies presented in previous chapters based on the use of gold nanoparticles and nanostructures and on their interaction with light. For instance, previous research works have demonstrated the potential of small aggregates made of a few NPs as effective SERS substrates due to the high electric field that reside in the inter-particle gaps called „hot-spots” [41-46]. However, there is still an insufficient understanding as regards to the optimum number of coupled NPs and the inter-particle gaps which can ensure a maximum SERS activity. Primarily, it is important to understand if dimeric or trimetric assemblies would be substantially more effective as SERS substrates than linear chains containing several NPs (>4). Such an answer is relevant from the experimental point of view as longer chains would not be easily fabricated, stabilized or directed in bio sensing applications. Secondly, a predictable spectral position for LSPR band of NPs arrangement would be helpful in selecting the right laser line needed for excitation to optimize the electromagnetic enhancement in SERS. Therefore, better understanding and rational optimization of collective plasmonic properties of linear chains as function of number and distance between NPs would be highly desirable.

Here, we report a theoretical analysis on the far- and near-field plasmonic properties of linearly assembled gold NPs. The analysis is based on comprehensive electromagnetic FDTD simulations, i.e. numerically solving Maxwell’s equations by iteration over time [47].

5.2 Theory and experiment

FDTD method

In order to predict the near- and far-field optical properties of metallic nanoparticles, it is necessary to solve a set of four partial differential equations known as Maxwell’s equations which describe the electric and magnetic components of the electromagnetic wave in interaction with quasi-free charges existing in metallic NPs. The FDTD is one of the most popular numerical methods to solve Maxwell’s equations for complex arrangement of nanoparticles that cannot be approached analytically. In present work, a commercial program from Lumerical [48] is used to investigate the plasmon resonances properties of linear chains of gold NPs. The approach of the FDTD method is that of dividing the physical space into small cubic cells, Yee cells (Figure 13A). Starting with some guess values, the electric fields are calculated on the edges of the cube and the magnetic fields crossing the faces using Maxwell’s equations. After

these first order approximation values are found, they are introduced in Maxwell's equations to obtain the second order approximation and continue this process until convergent results are obtained.

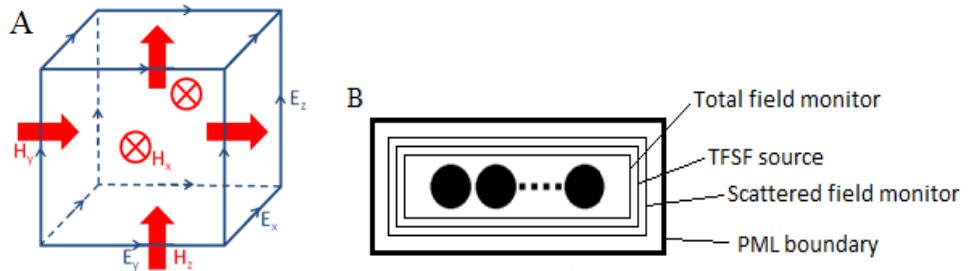


Fig. 1. (A) Yee cell representation; (B) Representation of the monitors, source and boundary conditions used in our simulations [47].

In all our simulations we have used a mesh of 0.5 nm because we found out that this is small enough to meet the convergence criteria, the far-field response being identical to simulations with mesh 0.2 nm or even 0.1 nm. To model the complex permittivity of gold, we used the experimental data of Johnson and Christy [49]. The source was a Total Field Scatter Field (TFSS), one that uses plane waves, suitable for problems concerning the scattering of small particles. We used power monitors arranged in such a way that we formed small boxes, one inside the TFSS source for the calculation of the absorption coefficients and one that contained the source for the scattering coefficient (see Figure 13B).

To probe both the longitudinal and transverse plasmonic response of NPs chain, the incident plane wave was considered either polarized parallel to the interparticle axis or perpendicular to this axis (Fig. 14).

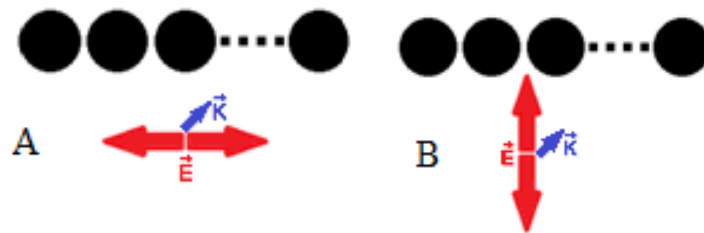


Fig. 14. The two polarizations of the incident wave: (A) electric field parallel to the interparticle axis and (B) electric field perpendicular to the interparticle axis [47].

Numerical simulations were performed on chains containing different numbers of spheres for each polarization presented above and results combined to depict the “unpolarised” LSPR spectrum.

5.3 Experimental: Synthesis and characterization of gold NPs

In this work spherical gold nanoparticles were synthesized according to the Turkevich-Frens method [50] by the aqueous reduction of HAuCl_4 with trisodium citrate.

To induce assembly of gold nanoparticles, 1 ml of aqueous colloidal solution was mixed with 500 μl of ethanol. 0.2 mM Pluronic F127 polymer was added at different periods of time (0, 15, 30, 50 s) to as prepared colloidal solution in order to stabilize the formed aggregates in solution.

Extinction spectra of colloidal solutions with different degree of aggregation were recorded using a Jasco V-670 UV-Vis-NIR spectrometer with a slit width of 2 nm and 1 nm spectral resolution. The NPs assemblies were examined using a JEOL 100 U type transmission electron microscope operated at 100 kV accelerating voltage.

5.4 Comparison with experimental spectra and discussion of the results

Fig. 15A shows a sequence of simulated LSPR spectra corresponding to increasing number of NPs in chains with constant inter-particle distance of 0.5 nm. While important red-shifts of LSPR band assigned to longitudinal coupling can be noticed only minor red-shifts occur for LSPR bands assigned to transversal polarization as compared to spectrum of individual NPs.

More interestingly, we found that the spectral position of LSPR band assigned to longitudinally coupled NPs can be described by a sigmoid function $y(x)$:

$$y = A_2 + (A_1 - A_2) / (1 + (x/x_0)^p)$$

where y and x represents the spectral position of band and number of NPs in the chain, respectively.

In the above equation A_1 , A_2 , x_0 and p are fitting parameters. The value $A_2=739\text{nm}$ is obtained from a simulation considering an infinite chain while other parameters can be obtained by fitting considering $y=616\text{nm}$ for $x=2$ ($A_1=525\text{nm}$, $x_0=2.601$ and $p=1.04$ and the correlation coefficient $R=0.982$) [47]. Based on this equation it is possible to predict the wavelength at which a chain composed of a given number of spheres exhibits the maximum LSPR.

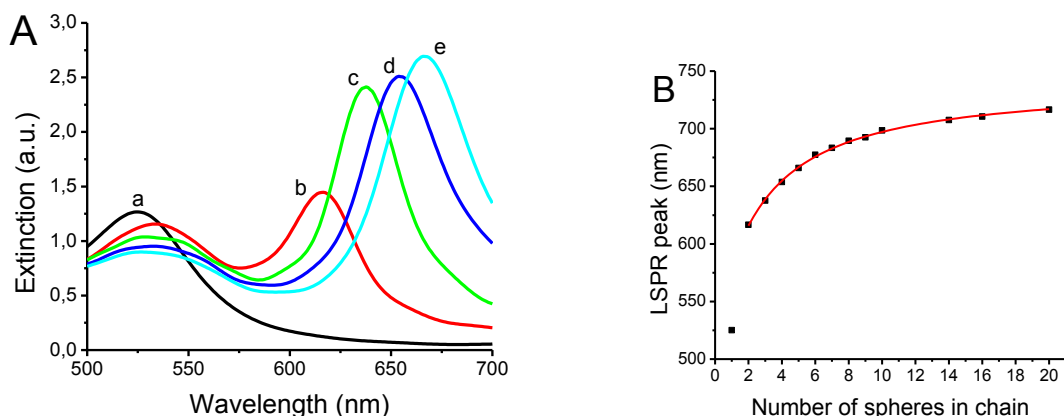


Fig. 15. (A) Simulated LSPR spectra of chains of gold NPs of 20 nm diameter and interparticle distance of 0.5 nm surrounded by water ($n=1.33$) and composed of 1 (a-black), 2 (b-red), 3 (c-green), 4 (d-blue) and 5 (e-cyan) NPs. (B) LSPR spectral position as function of the number of particles in the chain [47].

The analysis of TEM pictures recorded after stabilization of colloidal solution is the usual way to provide the histogram of distribution of monomers, dimers, trimers, etc. existing in colloidal solution (Fig. 16C). However, alternative methods to provide some similar information about the size of chains and their distribution in a colloidal solution extracted from their LSPR spectra would be highly desirable.

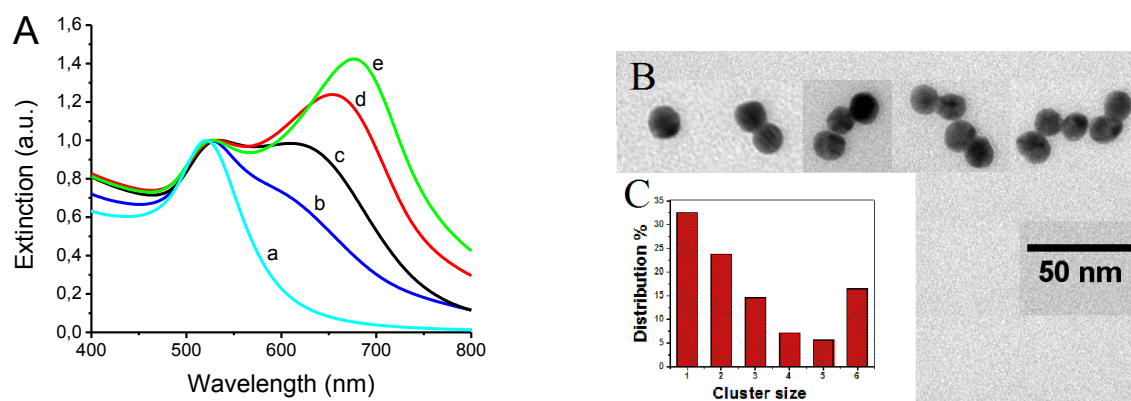


Fig. 16 (A) Normalized extinction spectra recorded from colloidal solutions with various degree of aggregation. The measurements proceeded at various time intervals after adding of polymer to solution (0 s – blue, 15 s – black, 30 s – red and respectively 50 s – green). For reference the spectrum of non-aggregated solution is given in cyan. (B) Representative TEM pictures of chains formed in solution. (C) Histogram of chain lengths distribution in solution after immediate adding of Pluronic [47].

The results obtained demonstrate that the experimental, composite LSPR spectrum recorded from a colloidal solution of a certain degree of aggregation can be analysed with a “trial

and error” method based on linear combination of theoretical spectra computed above for chain of different lengths. Indeed, the analysis of the experimental spectrum (Figure 16 A, spectrum b) provides the percentage of monomers, dimers, trimers, etc. (see data in Table 1) which are consistent with the histogram provided by TEM pictures.

NPs/ chain Sample /method		1	2	3	4	5	6	7	> 7
		b	TEM	32.5	23.6	14.6	7	5.6	-
	Fit	28.2	25	9.1	4.5	3.4	0.9	0.8	28
c	Fit	2.4	39.8	12.1	12.3	6	0.6	0.6	26
d	Fit	0.6	22.6	14.2	14.9	16.2	3.4	2.6	25
e	Fit	0.4	17.5	11	11.7	12.5	7	18.6	21.2

Table 1. Percentage of chains of different lengths existing in the colloidal solutions as provided by TEM (sample b) and “trial and error” method (samples b, c, d, and e) [47].

Therefore we can use the results provided by a “trial and error” method as first indicator for the “composition” of aggregated samples c, d and e (corresponding spectra are presented in Figure 16A) for which we do not provide TEM data.

Fig. 17A shows the experimental spectra together with spectra reconstructed by linear combination of above simulated spectra for chains of different lengths (see Figure 15A). As can be seen the reconstructed spectra feature much better spectral resolution of longitudinal and transversal bands relative to the experimental spectra which show bands much broader.

As shown in Figure 17 B, the LSPR band blue shifts and gradually reduces its intensity as the interparticle distance increases from 0.5 nm to 20 nm. [47]. Moreover, we can notice that for distances larger than 15 nm, the profile of extinction spectrum is almost identical with that of isolated NP. The limit of 0.5 nm between NPs is the lowest possible one that we could simulate due to computational restrictions. However, for a smaller separation distance the contribution of the quantum tunnelling effect increases and the classical electrodynamics theory is no longer an accurate approximation [51, 52].

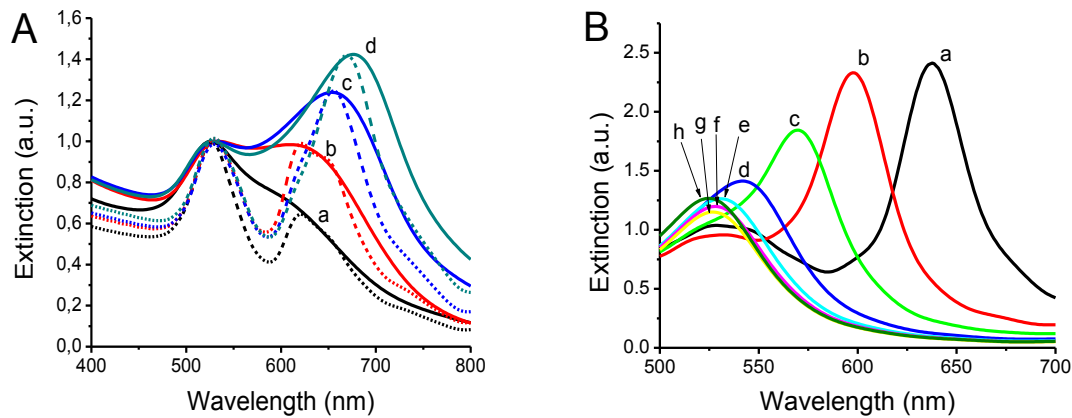


Fig. 17. (A) Experimental spectra (continuous line) together with theoretical spectra reconstructed by linear combination of above simulated spectra for chains of different lengths. (B) Simulated LSPR spectra of chains composed of three gold nanoparticles of 20 nm diameter for different interparticle distances 0.5 nm (a-black), 1 nm (b-red), 2 nm (c-green), 5 nm (d-blue), 10 nm (e-cyan), 15 nm (f-magenta), 20 nm (g-yellow) and, as reference, single isolated sphere (h-olive) [47].

In the above simulations the chains were considered to be perfectly aligned. However, as can be seen in the TEM image, some deviations from the linear chain-like structure could exist. Therefore a series of simulations were performed to reveal the optical response of non-perfectly aligned chains and estimate their contribution to overall spectra recorded from the colloidal solution.

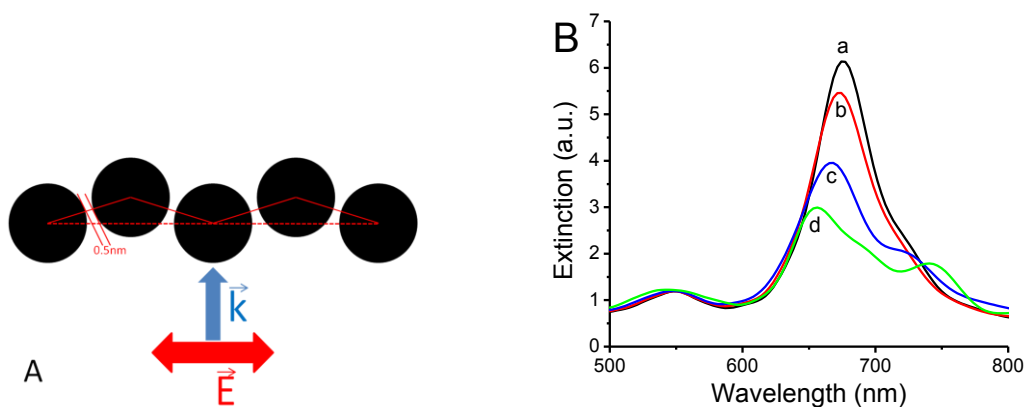


Fig. 18 (A) Top-view schematic of the geometry of the chains with different angles between adjacent NPs. (B) Simulated extinction spectra obtained from 5 sphere chains with different angles (0 degrees - a, 10 degrees - b, 20 degrees - c and 30 degrees - d) between the NPs in water ($n=1.33$) with an interparticle distance of 0.5 nm [52].

For simulation we consider a gradual variation of the deviation angle within the range 0-30 degrees, while keeping the inter-particle distance fixed at 0.5nm. The computed spectra for deviation angles of 0, 10, 20 and 30 degrees are plotted in Figure 18B. As function of increasing angle, the main longitudinal surface plasmon resonance decreases in intensity and shifts toward blue revealing a second multipolar resonance located in the red side. It is conceivable that such effects can explain at least partially the broad feature of experimental spectra when compared to reconstructed spectra generated only by linear chain-like structure.

5.5 Theoretical calculation of position, shape and of electromagnetic field of plasmonic resonances generated by nanoparticles chains

Apart from the far-field optical properties of the gold NPs chains we were interested to analyze the electrical field intensity (E^2) at the surface of NPs in a plane perpendicular to the propagation direction of the waves that contains the NPs centres. For simulation we considered light polarized parallel to the interparticle axis. The maps represent the distribution of logarithmic values of electrical field intensity normalized to the incident field E_0^2 considered equal to unity ($\log(E^2/E_0^2)$).

As we can see in Fig. 19, the highest field intensity is always located in the middle of the chain, either in the central gap in the case of chains composed of even number of spheres or at the interstices between the central sphere and its two neighbours for chains composed of odd number of spheres.

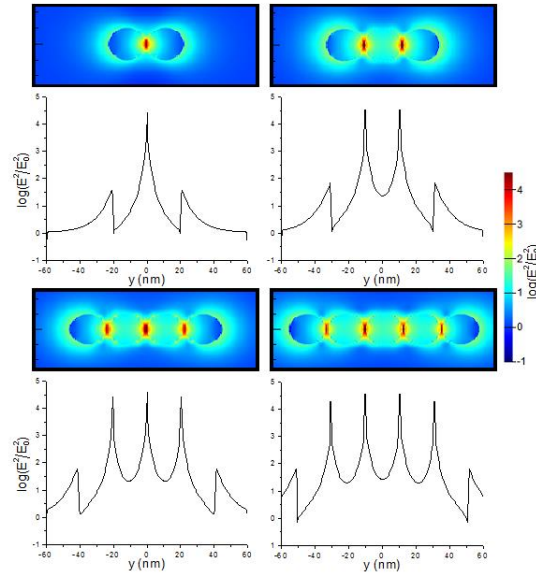


Fig. 19. Maps of electric field enhancement ($\log(E^2/E_0^2)$) in the XOY plane for chains composed of different number of NPs. A cross-section representation of field enhancement is given for each map [47].

Fig. 20A presents a plot of the maximum enhancement factor ($\log(E^2/E_0^2)$) for the intensity of the electric field as function of different number of spheres. We can observe that the maximum enhancement is reached for a chain composed of 4 NPs. This can be explained taking into consideration that the minimum of damping coefficient for gold coincides with LSPR wavelength for the chain of 4 sphere chain (655nm) as can be seen in figure 20B [47]. . For comparison we considered the case of chains in a surrounding medium with refractive index $n=1$ (air). Unlike chains in water, in the case of air the field enhancement increases toward a saturation level. For an infinite number of spheres the saturation level in water is the smallest of all chain lengths simulated whereas for air it is the highest. This observation can be attributed to the fact that the extinction peak for the infinite chain of spheres in air is at 620 nm, where the damping function is still decreasing at this wavelength.

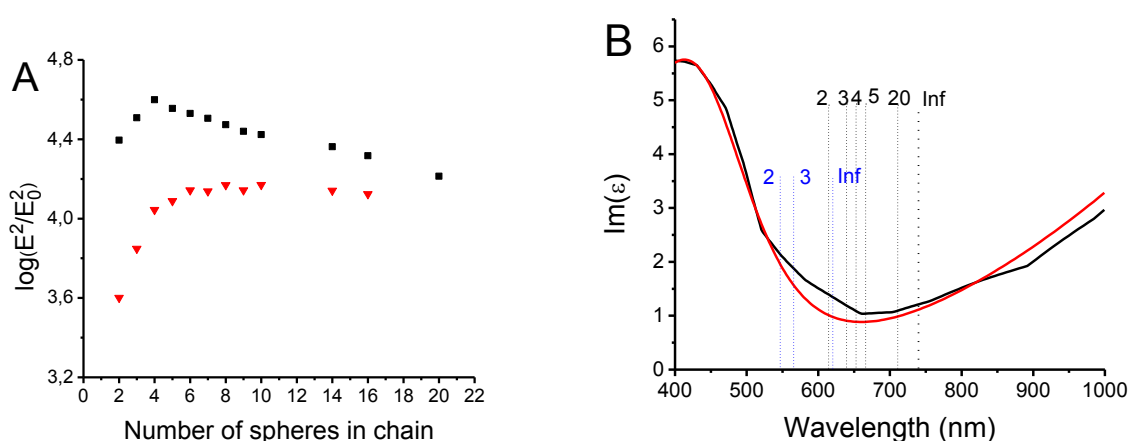


Fig. 20 (A) Plot of logarithmic intensity maximum of the normalized electric field as function of the number of spheres in the chain. The spheres are of 20 nm diameter and separated by 0.5 nm. The black squares are for water ($n=1.33$) and the red triangles are for air ($n=1$) as surrounding media. (B) The imaginary part of the electric permittivity of gold (black line – Johnson and Christy) and fitted by the FDTD program (red line). Also depicted are the LSPR positions for chains of different number of NPs in water (black vertical dotted lines) and in air (blue vertical dotted lines) [47].

Figure 21 represents a few examples of logarithmic distributions of the electrical field intensity in the case of trimers with different interparticle distances. As we can see for the $d=0.5$ nm case, we obtained $E^2/E_0^2 \approx 10^{4.6}$, which accounts for an electromagnetic enhancement of approximately 10^9 if you would use it as a SERS substrate, which is a promising result for applications [47].

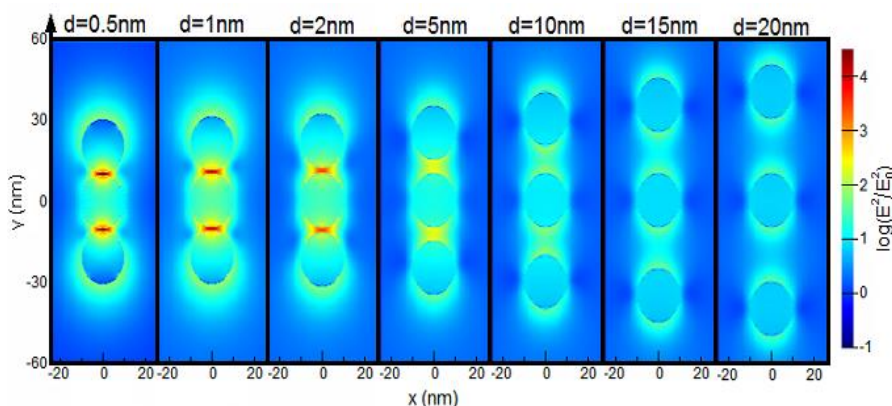


Fig. 21. Maps of logarithmic distribution of the electric field intensity surrounding chains of 3 gold nanospheres of 20 nm diameter in a medium with $n=1.33$ for different interparticle distances: 0.5, 1, 2, 5, 10, 15, 20 nm. All plots are calculated at the LSPR wavelength [47].

Chapter 6

Final conclusions and perspectives

Final conclusions

Experimental and theoretical studies performed in this doctoral thesis led me to these final conclusions:

1. I identified a made of gold nanoparticles covered with RhB molecules which may function as a spectroscopic transducer in the presence of the zinc ions in solution. *More exactly, I validated a transduction mechanism based on switching the fluorescence emission from the “off” state (when the molecule is adsorbed on the nanoparticle’s surface and there are no zinc ions in solution) in the “on” state (corresponding to the situation when we put ions in solution which move the RhB molecule from the nanoparticle’s surface).*
2. I calibrated the hybrid fluorescence sensor “nanoparticle-molecule”, finding a linear dependence between the fluorescence intensity and the Zn^{2+} ions concentration in a large domain of concentrations.
3. The SERS method, though is very well known in the literature for its capacity of highlighting infima quantities of organic molecules through their Raman spectra, still poses a few problems regarding the feasibility of plasmonic substrates. Therefore, production of the plasmonic substrates, active in near-infrared (NIR), a domain where the fluorescence background of the majority of the organic contaminants is small, which must be stable in time and to provide reproducible measurements is still unsolved. *For example, in my second study we managed to*

produce and test a new plasmonic substrate, which proved to be very SERS active at the laser's wavelength in NIR domain, at 785 nm. This substrate consists of tri-dimensional networks of gold nanowires that I obtained starting with the fundamental ingredients used in the previous study through the control of assembly and fusion of gold nanoparticles in the presence of a specific concentration of zinc ions in solution.

4. The substrate thus obtained was validated as an efficient SERS substrate on three molecular species (para-aminothiophenol, basic fuchsine, methylene blue), establishing the limit of detection in the domain 3×10^{-8} M.

5. In the third study I implemented the FDTD method which allowed us to analyse theoretically the interaction of the light with networks of gold nanoparticles assembled linear or nonlinear. *More exactly, we obtained the plasmonic resonance spectra and the values of the electromagnetic near-field at the nanoparticles' surface, corresponding to a chain consisting of an increasing number of nanoparticles and I compared them with the experimental extinction spectrum.*

6. We established an empiric formula which allows the direct calculation of the position of the LSPR band as a function of the number of the particles in the chain.

7. With direct relevance for SERS, we discovered that the maximum enhancement factor of local electric field is obtained for a chain composed of a number of four nanoparticles and the increasing of the distance between nanoparticles has as a result the decrease of the amplification of the field and the resonances blue-shift and diminish in intensity, until they reach the limit case of the plasmonic resonance of one single nanoparticle

Perspectives

1. The extension of the study for could be the use of the hybrid fluorescence sensor “nanoparticle-molecule” for the specific detection of other types of metallic ions.

2. The extension of the study for could be the use of network gold nanowires for the implementation of SERS multiplex detection (simultaneous detection and identification of many organic pollutants);

3. The transfer of the results of these laboratory studies in new types of sensors for use in real situations.

Selected references

- [1]. M.C.Daniel, D.Astruc, *Chem. Rev.*, 104, 2004, 293
- [2]. G. Mie, *Ann. Phys.*, 25, 1908, 377
- [3]. A. P. Alivisatos, *Science*, 271, 1996, 933
- [4]. A. Henglein, *J. Phys. Chem.*, 97, 1993, 8457
- [5]. K. L. Kelly, E. Coronado, L. L. Zhao, G. C. Schatz, *J. Phys. Chem. B*, 107, 2003, 668
- [6]. A. L. Gonzales, C. Noguez, *J. of Comput. And Theoret. Nanoscience*, vol. 4, 2007, 231
- [7] A. Mooradian, *Phys. Rev. Lett.*, 22, 1969, 185
- [8] J. P. Wilcoxon, J. E. Martin, F. Parsapour, B. Wiedenman, D. F. Kelley, *J. Chem. Phys.* 108, 1998, 9137
- [9] K. A. Willets, R. P. Van Duyne, *Ann. Rev. Phys. Chem.*, 58, 2006, 267
- [10] E. Hutter, J. H. Fendler, *Adv. Mater*, 16, 2004, 1685
- [11] K. Hamamoto, R. Micheletto, M. Oyama, A. A. Umar, S. Kawai, Y. Kawakami, *J. Opt. A*, 8, 2006, 268
- [12] J. R. Lakowicz, *Principles of Fluorescence Spectroscopy*, Kluwer Academic/Plenum Publishers, 1999
- [13] T. W. Collette, T. L. Williams, *J. Environ. Monit.*, 4, 2002, 27
- [14] M. F. Fleischman, P. J. Hendra, A. J. Millan, *Chem. Phys. Lett.*, 26, 1974, 163
- [15] C. L. Haynes, A. D. Mc Farland, R. P. Van Duyne, *Annal. Chem.* 1, 2005, 339A
- [16] E. J. Zeman, G. C. Schatz, *J. Phys. Chem.*, 91, 1987, 634
- [17] T. Iliescu, D. Maniu, S. C. Pînzaru, R. Grecu, S. Aştilean, *Aplicații ale spectroscopiei vibraționale*, Ed. Casa cărții de știință, Cluj-Napoca, 2002
- [18] – D. S. Țîra, M. Focșan, S. Ulinici, S. Aştilean, *Spectroscopy Letters*, Volumul 47, No. 2, (2014), 153
- [19] – M.Baia, F.Toderaș, L.Baia, J.Popp, S.Aştilean, *Chem. Physics Letters*, 422, 2006, 127
- [20] – E.Hutter, J.H. Fendler, *Adv.Mater.*, 16, 2004, 1685
- [21] – G.K. Darbha, A. Ray, P.C. Ray, *ACSNANO*, Vol.1, No.3, 208
- [22] – M.Stobiecka, M.Hepel, *Phys.Chem.Chem.Phys.*, 13, 2011, 1131
- [23] V. Rocher, J.M. Siaugue, V. Cabuil, A. Bee, *Water Res.* 42, 2008, 1290-1298.
- [24] M.C. Wu, M.P. Lin, S.W. Chen, P.H. Lee, J.H. Lic, W.F. Su, *RSC Adv.* 4, 2014, 10043-10050.
- [25] Z. Gan, A. Zhao, M. Zhang, W. Tao, H. Guo, Q. Gao, R. Maa, E. Liua, *Dalton Trans.* 42, 2013, 8597–8605.
- [26] R.F. Aroca. *Surface enhanced vibrational spectroscopy*, 2006, New York: Willey.

- [27] M. Baia, S. Astilean, T. Iliescu, Raman and SERS investigations of pharmaceuticals, 2008, Berlin:Springer.
- [28] Z. Wang, L. W. Rothberg, *J. Phys. Chem. B* 109, 2005, 3387-3391.
- [29] D. S. Țîra, M. Potara, S. Aștilean, *Materials Research Bulletin*, Vol. 64, 2015, 267-273
- [30] J. Turkevich, P. C. Stevenson, J. Hillier, *Discuss. Faraday Soc.* 11, 1951, 55–75
- [31] K.P. Jain, I.H. El-Sayed, L. K. Seok, M.A. El-Sayed. *J. Phys. Chem. B* 110, 2006, 7238-7248.
- [32] C. H. Munro, W. E. Smith, M. Garner, J. Clarkson, P. C. White, *Langmuir* 11, 1995, 3712-3720.
- [33] L. Marsich, A. Bonifacio, S. Mandal, S. Krol, C. Beleites, V. Sergo, *Langmuir* 28, 2012, 13166–13171.
- [34] I. A. Larmour, E. A Argueta, K. Faulds, D. Graham, *J. Phys. Chem. C* 116, 2012, 2677–2682.
- [35] X. Zou, S. Dong, *J. Phys. Chem. B* 110, 2006, 21545–21550.
- [36] Z. Sun, C. Wang, J. Yang, B. Zhao, J. R. Lombardi, *J. Phys. Chem. C* 112, 2008, 6093–6098.
- [37] G.N. Xiao, S.Q. Man, *Chem. Phys. Lett.* 447, 2007, 305–309.
- [38] T. Simon, S. C. Boca, S. Astilean, *Colloids Surf. B: Biointerfaces* 97, 2012, 77– 83
- [39] H. B. Lueck, D. C. Daniel, J. L. McHale, *J. Raman Spectrosc.* 24, 1993, 363-370.
- [40] X. Zhou, F. Zhou, H. Liu, L. Yang, J. Liu, *Analyst*, 138, 2013, 5832-5838
- [41] J.A. Schuller, E.S. Barnard, W. Cai, Y.C. Jun, J.S. White, M.L. Brongersma, *Nat. Mater.* 9, 2010, 193.
- [42] T. Chung, S.Y. Lee, E.Y. Song, H. Chun, B. Lee, *Sensors* 11, 2011, 10907.
- [43] Z. Zhu, T. Zhu, Z. Liu, *Nanotechnology* 15, 2004, 357.
- [44] N.J. Halas, S. Lal, W.S. Chanq, S. Link, P. Nordlander, *Chem. Rev.* 111, 2011, 3913.
- [45] K.A. Willets, R.P. Van Duyne, *Annu. Rev. Phys. Chem.* 58, 2007, 267.
- [46] J.Z. Zhang, C. Noguez, *Plasmonics* 3, 2008, 127.
- [47] C. A. Țîra, D. S. Țîra, T. Șimon, S. Aștilean, *Journal of Molecular Structure*, Vol. 1072, (2014), 137-143
- [48] http://docs.lumerical.com/en/fdtd/knowledge_base.html. [Online] Lumerical Solutions, Inc.
- [49] P.B. Johnson, R.W. Christy, *Phys. Rev. B* 6, 1972, 4370.
- [50] G. Frens, *Nat. Phys. Sci.* 20, 1973, 241.
- [51] R. Esteban, A.G. Borisov, P. Nordlander, J. Aizpurua, *Nat. Commun.* 3, 2012, 825.

[52] J.G.F. Abajo, J. Phys. Chem. C 112, 2008, 17983.

LIST OF PUBLICATIONS

I. Articles in ISI journals, related to thesis:

1. **Daniela Simona Țîra**, Monica Focșan, Sorin Ulinici, Simion Aștilean, *Rhodamine B-coated Gold Nanoparticles as Effective Turn-On Fluorescent Sensors for Detection of Zn²⁺ Ions in Water*, Spectroscopy Letters, Volumul 47, No. 2, (2014), 153-159 (7pp) (IF =0.67) <http://dx.doi.org/10.1080/00387010.2013.782557>

2. **Daniela Simona Țîra**, Monica Potara, Simion Aștilean, *Fabrication of Stable Network-like Gold Nanostructures In Solution and Their Assessment as Efficient NIR-SERS Platforms for Organic Pollutants Detection*, Materials Research Bulletin, Vol. 64, (2015), 267-273 (IF=1.913) <http://authors.elsevier.com/a/1QKJa5pgl9M-p>

3. Cristian Țîra, **Daniela Simona Țîra**, Timea Șimon, Simion Aștilean, *Finite-Difference Time-Domain (FDTD) Design of Gold Nanoparticle Chains with Specific Surface Plasmon Resonance*, Journal of Molecular Structure, Volumul 1072, (2014), 137-143 (IF=1.404)

II. Articles in ISI journal, unrelated to thesis:

Sorin Claudiu Ulinici, **Daniela Simona Țîra**, Grigore Vlad, Dumitru Vaju, *Experimental Study and Numerical Modeling of the Water/Ozone Contact Systems In The Bubble Column*, Environmental Engineering and Management Journal, Volumul 12, (2013), No. 3, 503-508 (IF=1.004)

III. Articles in non - ISI journals:

1. **Daniela Simona Țîra**, Monica Potara, Felicia Toderas, Sorin Claudiu Ulinici, Simion Aștilean, *Detection Of Zn²⁺ Ions In Water By Local Surface Plasmon Resonance (LSPR) Sensors*, **Studia Universitatis Babes-Bolyai Physica**, LIII 1, (2008), 93-99

2. Sorin Ulinici, Suci Liviu, **Daniela Simona Țîra**, *Considerații privind proprietățile antibacterieneale suprafețelor nanostructurate de argint*, **Environment & Progress**, No.12, 2008, 487-496

3. **Daniela Simona Țîra**, Sorin Claudiu Ulinici, Simion Aștilean, *Fluorescence Sensors for Detection Of Zn²⁺ Ions In Water*, **Ecoterra**, no. 25, 2010, 185-190.

Acknowledgements

First of all I would like to express my gratitude to all those who helped me with the publication of this work. I thank God who makes all things possible. I also want to thank my family, my husband Vasile and my son, Cristian Alexandru, for their love, patience and

encouragements they offered me during this period. My thanks address equally to my parents for their trust in me, for their moral support, encouragements, patience and help they gave me during my professional growth.

I thank my scientific advisor, Prof. Dr. Simion Aștilean, for introducing me in the field of Nanotechnology, for counselling me and his permanent moral support. I also thank Conf. Dr. Dana Maniu, Conf. Dr. Monica Baia și Prof. Dr. Mihai Todica for their useful and relevant observations and their support.

I also thank my colleagues from Nanobiophotonics Centre, Dr. Monica Potara, Dr. Monica Foçșan, Dr. Sanda Boca, Dr. Felicia Toderaș, Drd. Cristian Alexandru Țîra from whom I learned a lot during my activity in the optic laboratory.

I express my gratitude to my referees, Prof. Dr. Dana Dorohoi and Prof. Dr. Ioan Bratu for their valuable time they spent to read this thesis, for their observations and suggestions.

Some nice results in my thesis couldn't be achieved without the handful help of Dr. Lucian Barbu-Tudoran, Drd. Cristian Alexandru Țîra Dr. Monica Potara, Dr. Monica Foçșan, Dr. Sanda Boca, și Drd. Sorina Suărășan.

The work described in chapter 3 was supported by CNCSIS-UEFISCSU, projects number PNII_ID_PCCE_312/2008.

The work described in chapter 4 was supported by CNCSIS-UEFISCSU, projects number PNII_ID_PCCE_129/2008.

The work described in chapter 5 was supported by CNCSIS-UEFISCSI, projects number PNII_ID_PCCE_129/2008 and by Babeș-Bolyai University, GTC_34015/2013.